POLITECNICO
MILANO 1863

SCUOLA DI INGEGNERIA INDUSTRIALE
E DELL'INFORMAZIONE

Executive Summary of the Thesis

Characterization of Fragmentation Events in Near Earth Environment exploiting Conjunction Analysis

Laurea Magistrale in Space Engineering - Ingegneria Spaziale

Author: Paola Grattagliano

Advisor: Prof. Marco Felice Montaruli

Co-advisor: Prof. Pierluigi Di Lizia

Academic year: 2022-2023

1. Introduction and Scope

The ongoing rise in the number of orbiting Resident Space Objects (RSOs) is a significant concern in the advancement of space services, particularly within the Low Earth Orbit. This population poses a threat to future missions and active satellites. When a debris impacts a functioning spacecraft, it can lead to the proliferation of additional fragments, triggering chains of potential collision events. These collisions may end the operational life of a satellite (or parts of it), causing scientific and economic damage to any mission. The former effect however is the most critical: fragmentation events are in fact currently the dominant source of space debris [1]. The timely monitoring of the mentioned break-up events is of paramount importance to achieve fast and accurate forecast of the fragments trajectories. However, accomplishing this entails prior characterization of the event, including correlating the observed fragment to the correct parent object and detecting the event epoch. Various approaches are present in the literature for the estimation of the fragmentation epoch. The approach in [2] relies on statistical distance metrics, the one in [3] on the analysis of the orbital elements of fragments over time, and ultimately [4] on the search for the minimum distance between single objects and the fragments cloud centre. All of these methods make use of a set of Two-Line Elements (TLEs) to identify the parent object, and require a substantial number of orbital states for the produced fragments. However, their availability is deemed an optimistic assumptions. Thus, in the context of this work, it is supposed that the epoch estimation is required shortly after the event is alerted, when even a single fragment ephemeris is known. This assumption is at the basis of the tool developed in [5], named Fragmentation Epoch Detector Algorithm (FRED), which serves as the inspiration for the research presented in this summary. FRED approach investigates the best distance metric for the fragmentation epoch detection, as better detailed in Sec. 2.

Starting from the motivations reported above, this research aims to address the following questions:

- Can Conjunction Analysis (CA) techniques be leveraged for the accurate detection of a fragmentation event epoch?
- Can CA techniques provide criteria to associate a detected object with the original one?

- Can the approach implemented in FRED be enhanced with alternative metrics, such as Probability of Collision (PoC), for the characterization of fragmentation events?

2. Fundamentals

Some of the most significant mathematical tools exploited in this work are here summarized.
The stochastic representation in this thesis is applied through the Gaussian Mixture Models (GMM), deemed a valuable compromise between the Gaussian approximation and the computational demand of Monte Carlo techniques. Its underlying concept is to approximate any Probability Density Function (PDF) through a weighted sum of N Gaussian PDFs with smaller covariances:

$$p(\boldsymbol{x}) \approx \sum_{i=1}^{N} \alpha_i p_g(\boldsymbol{x}; \boldsymbol{\mu}_i, \boldsymbol{P}_i) \qquad \sum_{i=1}^{N} \alpha_i = 1$$

The weights, means and covariance matrices of the i-th element are derived through available univariate splitting libraries, applied to the multivariate distribution of the orbital state. The splitting is performed along a single direction, chosen to be the highest uncertainty one. The latter is found to be the eigenvector corresponding to the highest eigenvalue of the initial covariance matrix made dimensionless (dividing the positional and velocity elements respectively by the trace of the positional and velocity sub-matrices). Once generated, each element of the GMM is propagated through the Unscented Transform (UT). The reduction of the approximation domain accomplished through this splitting enables to capture the shape of the final non-Gaussian distribution far more precisely than with the propagation of the initial Gaussian. This represents a benefit in cases of nonlinear dynamics and extended time windows.

The NASA Standard Break-up Model (SBM) ([6]) is exploited to model the fragmentation event and generate a certain number of objects from which fictitious measurements are derived. Specifically, the SBM allows to compute the orbital states of the fragments derived from the parent object involved in the tested scenario, from Eq. 1.

$$\begin{cases} \boldsymbol{r}^f = \boldsymbol{r}^p \\ \boldsymbol{v}^f = \boldsymbol{v}^p + \Delta\boldsymbol{v}_{SBM} \end{cases} \qquad \text{at } t_{event} \qquad (1)$$

The superscripts p and f refer respectively to the parent and fragment objects, while the positional state is labelled as $\boldsymbol{r}$ and the velocity vector as $\boldsymbol{v}$.

CA refers to the assessment of possible in-orbit collisions between two objects. The PoC is defined at the Time of Closest Approach (TCA), corresponding to the epoch of minimum distance between primary and secondary object in the encounter frame, or B-plane. The latter is represented in Fig. 1, together with the combined sphere, whose radius is named Hard-Body Radius (HBR), obtained by summing the respective hard-body radii of the two space objects, assumed in this context as spherical.

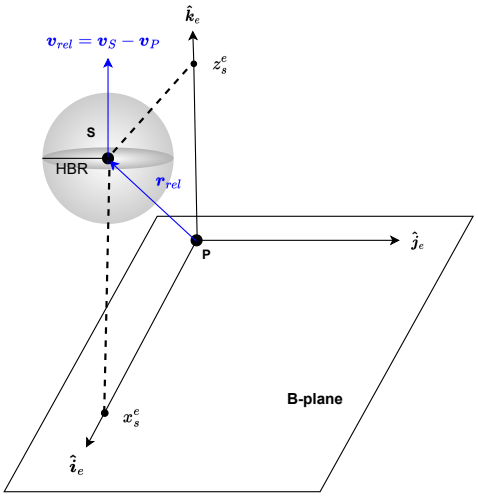

Figure 1: Primary (P) and secondary (S) objects in the encounter reference frame.

The underlying concept is the following: if at the TCA the mutual distance between the primary and secondary baricenters is smaller than the HBR, a collision occurs, and the PoC expresses the probability that this occurs, taking into account the position uncertainties. To compute the PoC value over the encounter period, the integral of the combined PDF shall be performed over the integration volume, which is a tube produced by the motion of the sphere encountering the *joint covariance ellipsoid* ([7]) centered on the primary RSO. This results in the following

triple integral:

$$P^c = \iiint_V p_g(\boldsymbol{x}_{TCA}; \boldsymbol{\mu}_{rel}, \boldsymbol{P}_C)\, dV$$

with the PDF assumed constant in time, and taken at TCA. $\boldsymbol{\mu}_{rel}$ denotes the mean relative position between the two objects and $\boldsymbol{P}_C = \boldsymbol{P}_P + \boldsymbol{P}_S$ is the combined covariance matrix of the relative position, owing to the assumptions of non-correlated position uncertainties.
Short-term conjunctions events are exploited in this research. In this case, a series of assumptions arise and simplify the calculation: the relative motion between two objects is uniform and rectilinear; the velocity uncertainty of the two objects can be neglected; the uncertainties on the position are assumed Gaussian, non-correlated for the two objects and constant during the encounter. Furthermore, assumptions of perfectly spherical shapes of the RSOs and single collision during the encounter are also included. These assumptions allow a further simplification: the integration tube is assumed infinite. This reduces the integration domain to the disk projection of the combined sphere onto the encounter plane and having radius equal to the HBR. Finally, a rotation from the encounter frame to the principal axes of the covariance matrix can be performed, achieving $(x^e, y^e) \rightarrow (x^u, y^u)$, such that the new coordinates (x^u, y^u) are along the major and minor axis. Both these simplification allow to eventually reduce the PoC computation to the following 2D integral:

$$P^c = \frac{1}{2\pi\sigma_x^u\sigma_y^u} \int_A \exp\left(-\frac{1}{2}\left(\frac{(x^u - x_s^e)^2}{(\sigma_x^u)^2} + \frac{(y^u - y_s^e)^2}{(\sigma_y^u)^2}\right)\right) dx\, dy$$

Its evaluation branches out into several approaches. Those implemented in the thesis and available for user selection are the analytical methods by Chan ([8]) and Serra ([9]), and Alfano's ([10]) numerical computation.

One of the fundamentals objectives of this work is to determine whether it is possible to enhance FRED [5] performance by employing alternative metrics for ranking candidate epochs, exploiting CA metrics. FRED approach is stochastic, as it is based on the statistical distance between two distributions involving the parent and the single fragment analyzed: the Minimum Orbital Intersection Distance (MOID) and the relative distance distributions. Fragmentation epoch candidates are first identified and then ranked according to this statistical distance, and the best fragmentation epoch is finally returned. The initial part of the routine implemented for this work draws inspiration from the MOID transit computation performed in FRED: in a very similar way, a set of candidates epochs are retrieved. However, the Monte Carlo approach exploited in FRED to model the fragment orbital state uncertainty is replaced by a statistical representation based on GMM, and differently from FRED this is performed also for the parent orbital state. In addition, the metrics applied to rank the candidate epochs switch to collision probability.

3. Algorithm implementation

3.1. Parent covariance association

For the parent object, a covariance matrix representing the uncertainty of the state obtained from the available TLE (a deterministic information) shall be first associated. In the work, the approach presented in [11] is exploited, which obtains both a covariance matrix and an autocorrelation function exploiting solely a set of publicly available TLEs in a time span of two weeks maximum. In this work a number of secondary $N_{tle} = 5$ is downloaded from Space-Track and used. This approach is applied to the TLE of the specific test case. The graphic result of this covariance generation is reported in Sec. 4.3, in Fig. 3, showing the benefits of this shape of the parent covariance matrix in the splitting phase.

3.2. Epoch detection algorithm

The first block of the routine (Fig. 2) computes a set of candidate epochs of possible encounters for each element i_p of the parent mixture $\{\boldsymbol{x}_{i_p}^p, \boldsymbol{P}_{i_p}^p\}$ and for each element i_f of the fragment mixture $\{\boldsymbol{x}_{i_f}^f, \boldsymbol{P}_{i_f}^f\}$. The ephemeris of the parent object is referred to as $\boldsymbol{x}^p$ and is dated to t_{tle}, epoch of the last TLE available before the event. The covariance matrix of the parent $\boldsymbol{P}^p$ is also dated to t_{tle} and associated to $\boldsymbol{x}^p$, following the approach presented in Sec. 3.1. The event is deemed to have occurred at $t_0 > t_{tle}$ and the related alert

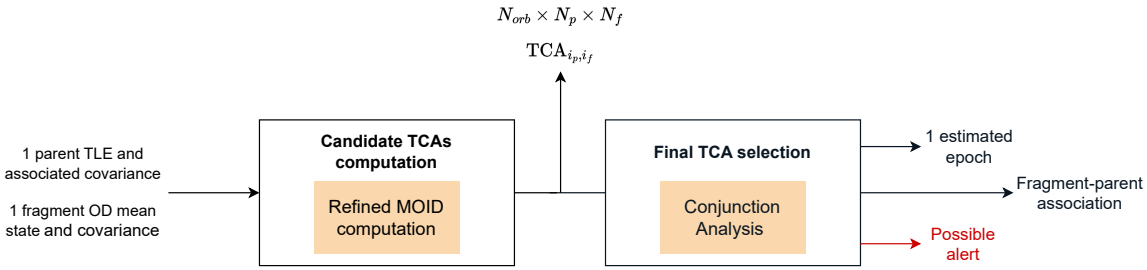

Figure 2: Routine flow chart.

notified at $t_a > t_0$. Some hours later, a fragment detection by a surveillance radar is simulated at $t_{od} > t_0$ [12] and its mean orbital state $\boldsymbol{x}^f$ and covariance matrix $\boldsymbol{P}^f$ are computed from an Orbit Determination (OD) process better detailed in Sec. 4.2. This first portion of the algorithm is structured as follows:

1. The window $[t_{tle}, t_a]$ is sampled with frequency $1/T_p$, T_p being the parent orbital period. This results in N_{orb} number of epochs t_i, each related to the i-th periodicity.
2. N_p and N_f Gaussian Mixture Elements (GMEs) are generated through the splitting approach described in Sec. 2. The state vectors $\boldsymbol{x}^p_{i_p}$ with $i_p = 1, ..., N_p$ and $\boldsymbol{x}^f_{i_f}$ with $i_f = 1, ..., N_f$ are produced.
3. A nested loop is started for each parent and fragment GME.
4. The mean states of parent and fragment GMEs are propagated to each t_i.
5. For each t_i, the MOID distance and its transit epochs are computed analytically (following [13]) for both elements i_p and i_f, leveraging Kepler's equation. Results are referred as $t^p_{i_p,i_f}$ and $t^f_{i_p,i_f}$. The i_p and i_f state vectors are propagated, possibly considering perturbations, up to $t^p_{i_p,i_f}$ and $t^f_{i_p,i_f}$ respectively, resulting in the orbital states $\boldsymbol{x}^p_{i_p}(t^p_{i_p,i_f})$ and $\boldsymbol{x}^f_{i_f}(t^f_{i_p,i_f})$, and the analytical and Keplerian computations of $t^p_{i_p,i_f}$ and $t^f_{i_p,i_f}$ are updated. Both epochs are iteratively modified in this manner until, between two consecutive steps, they do not change anymore (setting a tolerance of 1e − 03 s) [5]. This iterative process results in $N_{orb} \times N_p \times N_f$ couples of $\left(t^p_{i_p,i_f}, t^f_{i_p,i_f}\right)$ and $\left(\boldsymbol{x}^p_{i_p}(t^p_{i_p,i_f}), \boldsymbol{x}^f_{i_f}(t^f_{i_p,i_f})\right)$.
6. The fragment i_f state vector $\boldsymbol{x}^f_{i_f}(t^f_{i_p,i_f})$ is propagated up to $t^p_{i_p,i_f}$, resulting in $\boldsymbol{x}^f_{i_f}(t^p_{i_p,i_f})$. $t^p_{i_p,i_f}$ is selected instead of $t^f_{i_p,i_f}$ due to the higher reliability associated to the parent ephemeris.
7. To exclude unfeasible solutions, the $N_{orb} \times N_p \times N_f$ couples enter a filtering phase, applied on the epoch of parent element i_p transiting through the MOID ($t^p_{i_p,i_f}$). The first filter requires that the couples with combinations (i_p, i_f) for which $t^p_{i_p,i_f}$ is not included in the boundaries of the time window $[t_{tle}, t_a]$ are eliminated. With the second filter, for each t_i, the couples with combinations (i_p, i_f) for which $t^p_{i_p,i_f} < (t_i - T_p/2)$ or $t^p_{i_p,i_f} > (t_i + T_p/2)$ are filtered out. The last filter is based on a clustering algorithm (DBSCAN), applied to eliminate couples with combinations (i_p, i_f) considered outliers (setting the maximum time deviation to 5 minutes).
8. If $t^p_{i_p,i_f}$ related to all combinations (i_p, i_f) is not compliant for all of the periodicities, the fragment under analysis must be discarded.

For the fragments which are not discarded, the epochs of the element i_p transiting through the MOID are used as first guess to compute candidate TCAs, exploiting the orthogonality between the relative position and the relative velocity. The $N_{orb} \times N_p \times N_f$ candidate TCAs are found in correspondence of a null scalar product between position and velocity, through an optimization function and applying the Keplerian model. At this point each parent element i_p and fragment element i_f, expressed as the normal distributions $\{\boldsymbol{x}^p_{i_p}, \boldsymbol{P}^p_{i_p}\}$ and $\{\boldsymbol{x}^f_{i_f}, \boldsymbol{P}^f_{i_f}\}$ respectively, are propagated through an UT function to the final candidate TCA epochs.

The second block of the algorithm (Fig. 2), aims to finally detect the fragmentation event epoch. The inputs are obtained from the first portion of the routine and are thus processed using typical metrics of collision risk assessment. The event under analysis is treated as a conjunction

$$d_M\left(\mathrm{TCA}_{i_p,i_f}\right) = \left[\left(\boldsymbol{r}^f_{i_f}(\mathrm{TCA}_{i_p,i_f}) - \boldsymbol{r}^p_{i_p}(\mathrm{TCA}_{i_p,i_f})\right)\right]^T [\boldsymbol{P}^p_{i_p}(\mathrm{TCA}_{i_p,i_f}) + ... \\ \boldsymbol{P}^f_{i_f}(\mathrm{TCA}_{i_p,i_f})]^{-1} \left[\left(\boldsymbol{r}^f_{i_f}(\mathrm{TCA}_{i_p,i_f}) - \boldsymbol{r}^p_{i_p}(\mathrm{TCA}_{i_p,i_f})\right)\right] \quad (2)$$

between a primary object (the parent) and a secondary object (the fragment). The algorithm is structured as follows:

1. A nested loop is started for each parent and fragment GME.
2. For each t_i, the PoC between the current parent and fragment GMEs is computed, using one of the approaches mentioned in Sec. 2, or by default through Chan's method. The distributions $\{\boldsymbol{x}^p_{i_p}(\mathrm{TCA}_{i_p,i_f}), \boldsymbol{P}^p_{i_p}(\mathrm{TCA}_{i_p,i_f})\}$, $\{\boldsymbol{x}^f_{i_f}(\mathrm{TCA}_{i_p,i_f}), \boldsymbol{P}^f_{i_f}(\mathrm{TCA}_{i_p,i_f})\}$ at the corresponding candidate TCA epochs enter in the PoC computation. The covariance matrices are required solely in their positional components. The HBR of the combined sphere is also required, and shall be set by the user.
3. For each combination (i_p, i_f), N_{orb} collision probabilities are obtained ($P^c_{i_p,i_f}\left(\mathrm{TCA}_{i_p,i_f}\right)$). To locate a potential encounter in time, the periodicity and the corresponding TCA at which the computed probability is maximum are selected.
4. Overall, $N_p \times N_f$ TCA_{i_p,i_f} are hence obtained, retaining only those "selected" through the maximum PoC criterion. Only the couples mean-covariance corresponding to these TCA epochs are now considered.
5. A second statistical distance metric is applied. For each combination (i_p, i_f) the Mahalanobis distance $d_M\left(\mathrm{TCA}_{i_p,i_f}\right)$ is computed between the current parent and fragment GMEs as in Eq. 2, where the matrices $\boldsymbol{P}$ refer only here to the positional subcovariance.
6. Among all $N_p \times N_f$ values of $d_M\left(\mathrm{TCA}_{i_p,i_f}\right)$, the minimum is identified. The corresponding $\tilde{i}_p$ and $\tilde{i}_f$ indexes are selected, and the related epoch $\mathrm{TCA}_{\tilde{i}_p,\tilde{i}_f}$ is considered as the final estimated $\tilde{t}_0$. This implies to obtain a solution of the event epoch which corresponds to the closest distributions from the two mixtures, in terms of position.

3.3. Reliability criterion

A reliability criterion has been sought to assist operations following a fragmentation event. This should allow the routine to provide "alerts" whenever the epoch estimation for the observed fragment is not reliable. Drawing inspiration from the approach in [14], the measure of "peak contrast" is applied. The maximum PoC selection in the routine is considered reliable if the "peak" of the collision probability found as the highest is also distinct from the probabilities computed at other periodicities. In [14], the peak contrast is defined as the logarithmic ratio of the highest values of encounter probability:

$$P^c_{ratio} = \log_{10}\left(\frac{P^c_1}{P^c_2}\right) \quad (3)$$

In the algorithm developed in the thesis, when the maximum PoC value (P^c_1) is determined, the second highest (P^c_2) is also saved. The two values are inserted into Eq. 3, and if the resulting logarithm is less than a threshold, an alert is generated. This criterion serves to assess whether, with fixed elements i_p and i_f, there is a comparable collision probability at the refined TCAs in two different periodicities. In this case, either the larger PoC is still found at the periodicity where the event occurred, or, due to inaccuracies, the PoC value at a different periodicity slightly prevails. In the first case, the alert serves as a precaution. In the second case, the estimated epoch is wrong, however the operator is aware of the possible unreliability of the result.

3.4. Fragment-parent association

The second objective of the routine is to assess whether an observed fragment can be associated to the parent object involved in the event. To achieve this, a measure of cumulative collision probability is here proposed, as follows:

1. The PoC of an encounter at a certain epoch (P^c) is computed (through Vittaldev's approach [15] detailed below).

2. The probability that this encounter does not occur is computed as $(1 - P^c)$.
3. By repeating point 2 for the all the TCAs in the considered time span, and by evaluating their product $\Pi(1-P^c)$, the probability of no encounters happening within the considered time interval is retrieved.
4. The probability that at least one collision between the two objects occurs in the entire span can be now evaluated as: $P^c_{tot} = 1 - \prod_{i=1}^{N_{orb}}(1 - P^c)_i$.

The first step in point 1 involves acquiring a collision probability value for each potential encounter, that is for each candidate refined TCA. To accomplish this Vittaldev's formulation [15] is exploited, as in Eq. 4.

$$P^c = \sum_{i_p=1}^{N_p} \sum_{i_f=1}^{N_f} \alpha^p_{i_p} \alpha^f_{i_f} \left(P^c_{i_p,i_f} \left(\mathrm{TCA}_{i_p,i_f} \right) \right) \quad (4)$$

where $\alpha^p_{i_p}$ and $\alpha^f_{i_f}$ are the weights of the mixtures, derived from the univariate splitting library (Sec. 2). The PoC values at TCAs are computed as described in Sec. 3.2. Once the measure of total probability of collision P^c_{tot} is computed, it is compared to a threshold. If $P^c_{tot} <$ threshold, then the association of the fragment body to the primary object is not positive. Otherwise it may be said that the observed object is a product of the parent break-up.

4. Test case and results

All numerical simulations were run in Matlab, together with functions from NASA SPICE Toolkit. Moreover, a single core with Intel(R) Core(TM) i7-8565U CPU @ 1.80GHz 1.99 GHz processor was used.

4.1. Test case description

The considered fragmentation scenario concerns a kinetic Anti-Satellite test occurred at around 02:47 UTC on November 15th, 2021 [16]. This event led to the destruction of the Russian satellite Cosmos 1408, which is considered the parent object in the analysis. Its orbital elements are reported in Tab. 1.

4.2. Data set generation

The fragments data are first generated by applying the SBM (as described in Sec. 2). In particular, the parent state vector $\boldsymbol{x}^p = \{\boldsymbol{r}^p, \boldsymbol{v}^p\}^T$ at

$\boldsymbol{a}$ [km]	$\boldsymbol{e}$	$\boldsymbol{i}$ [deg]	$\boldsymbol{\Omega}$ [deg]	$\boldsymbol{\omega}$ [deg]
6844.7	0.002	82.7	123.3	134.5

Table 1: Cosmos 1408 Keplerian elements at 02:47 UTC on November 15th, propagated from t_{tle} through SGP4.

t_{tle} is propagated up to t_0: 02:47:00.000 UTC on November 15th, when the fragmentation event is modelled as a set of impulses applied to the orbital state, according to Eq. 1. In such way a set of 237 fragments is generated. Finally, the pericentre radius of each fragment is evaluated at t_0, and when its value corresponds to an altitude lower than 120 km, the fragment is discarded from further simulations, being expected to re-enter.

The obtained fragments ephemerides are propagated to epoch t_{od} (obtaining $\boldsymbol{x}^f(t_{od})$), when a surveillance radar detection is simulated. Nominally, t_{od} is set at 13 hours after the fragmentation event, to replicate the availability of a single fragment observation few hours after the break-up. The determination process now branches out: to assess the algorithm performance, both the scenario neglecting OD errors and involving them are investigated. In any case the final output is the couple mean state and uncertainty covariance for each single fragment $\{\boldsymbol{x}^f, \boldsymbol{P}^f\}$.

In the scenario with no OD error, a fixed covariance matrix (with standard deviations on position and velocity of respectively $9.32e-05$ km and $1.38e-06$ km/s) is simply associated to all fragments. This matrix is derived through the same Initial Orbit Determination (IOD) and Refined Orbit Determination (ROD) approaches detailed below, setting low values for the measurements noise.

In the scenario with OD error, the fragment mean state $\boldsymbol{x}^f(t_{od})$ is propagated in the measurement window $[t_{od}, t_{od} + 30\mathrm{s}]$. The resulting propagated states are projected in the measurements space to derive a set of simulated angular and range measurements. These are perturbed, generating random values according to the sensor accuracy covariance. A default noise on the range measurement is fixed to 30 m, while both azimuth and elevation noises are set to 0.01°, nominally. First, the IOD process reported in [17] is applied on them, and its result is refined through the ROD function in [18], return-

ing $\{\boldsymbol{x}^f, \boldsymbol{P}^f\}$ defined at $t_{od} + 30$ s.
The remaining inputs are defined. The analysis time window ranges from t_{tle} (2021-11-14 23:20:00.000 UTC) to t_a (2021-11-15 06:00:00.000 UTC). The number of parent and fragments GMEs is fixed to $N_p = N_f = 9$. The t_{od} epoch set to $t_0 + 13$h, resulting in $N_{orb} = 5$. The combined HBR is set equal to the sum of the parent HBR (2.5 m), and of the fragment HBR (characteristic length derived from the SBM). The time error of the estimated solution compared to the true fragmentation epoch is computed as:

$$\varepsilon = |t_0 - \tilde{t}_0| \tag{5}$$

For a single fragment analysis, the result is considered successful if the error in Eq. 5 is below a threshold quantity, set equal to 60 s. The lower bound of the reliability criterion P^c_{ratio} described in Sec. 3.3 is set equal to 0.6 in the simulation. Finally the minimum threshold of P^c_{tot} for a positive fragment-parent association, described in Sec. 3.4, is set to 10^{-9}.

4.3. GMM test case

To illustrate the benefit of using the GMM in the approach, the graphical representations resulting from the splitting applied to the parent covariance (estimated through the method mentioned in Sec. 3.1) are reported. In Fig. 3a the normal distribution of the parent position is represented both through a Monte Carlo distribution (in black) and GMEs (colored), considering 10,000 samples in both cases. It can be noticed that the two representations are compliant, as well as after Keplerian propagation to t_a, as reported in Fig. 3b. In particular, each GME is propagated through UT, allowing a lower computational demand.

4.4. Simulations results

For all fragments that do not yield a correct estimation ($\varepsilon > 60$ s), two categories can be identified. In the *selection failures* case, the algorithm converges to a periodicity outside of the correct one (i.e. the third one in the scenario analysed). In the *TCA failures* case, even though the convergence to the correct periodicity is always achieved, the error is anyway higher than a minute. This can be attributed exclusively to an estimation of the candidate TCA epochs which is less accurate,

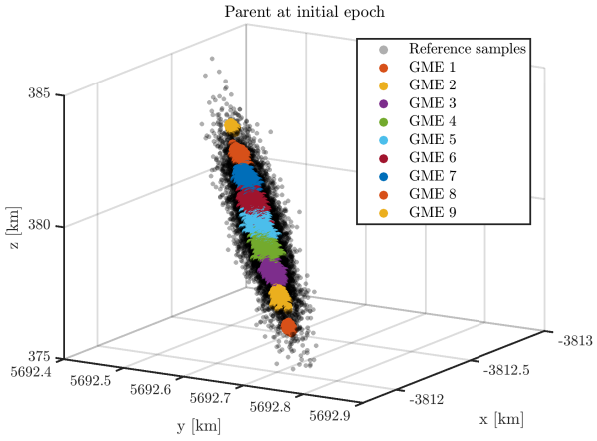

(a) Epoch t_{tle}.

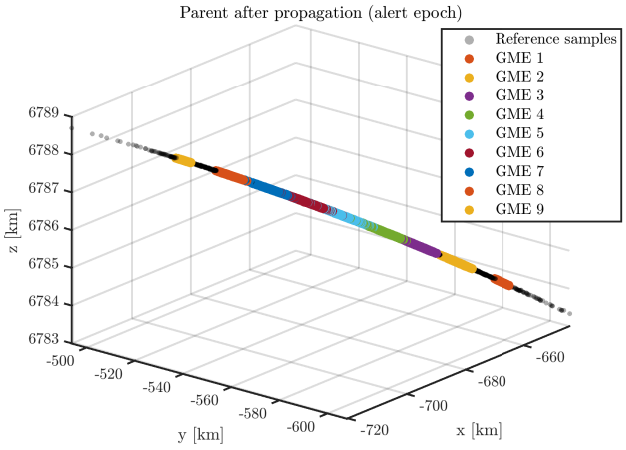

(b) Epoch t_a (after propagation).

Figure 3: Parent object GMEs. Positions in ECI frame.

and may occur due to the MOID computation or in the afterward refinement of the TCAs. The fragments percentage called *alerts* refers to those cases for which the reliability criterion described in Sec. 3.3 returns a value lower than the threshold.
The unperturbed scenario without OD error is first tested to assess the theoretical performance of the routine. The propagation in time, both in the data set generation and within the algorithms, occurs here through an analytical Keplerian model. The fragments detection is conducted with no error as reported in Sec. 4.2. In this case 229 fragments passed all filters; their results are reported in Tab. 2. All fragments estimate the event epoch with an error of less than a minute, even in the order of milliseconds. The fragment-parent association is also successful for all simulated fragments.

Case	Correct solutions	Selection failures	TCA failures	Alerts
Kep	100%	0%	0%	0%
SGP4	100%	0%	0%	0%

Table 2: Results for the scenarios with no OD error.

Equally good performances are obtained in the perturbed scenario (results in Tab. 2). The conversion inside SGP4 function from the Cartesian to TEME frame (and viceversa) is accomplished using a fixed-point iteration loop, introducing an error that accumulates along the propagation, potentially impacting on the results. However, in this scenario and looking at results in Tab. 2, it seems not affecting the outcome in terms of correctness of the solution. This is a positive outcome; however, numerical errors resulting from the conversion to SGP4 elements are reflected in the epoch estimates. These lead to errors (not reported here) in the order of milliseconds, but slightly higher than in the Keplerian case.
The routine shall be also tested under conditions that are as representative as possible of an operational scenario, hence it is necessary to introduce an error. This results in a perturbation of the fragments mean orbital state with respect to the ground-truth. Thus, their detection is performed here through the approach described in Sec. 4.2, introducing an error through the measurements noise covariance and the OD process. Results are reported for both the perturbed and unperturbed cases in Tab. 3. As evident, in the majority of cases, the

Case	Correct solutions	Selection failures	TCA failures	Alerts
Kep	82.5%	17.0%	0.5%	5.7%
SGP4	83.1%	16.9%	0%	5.8%

Table 3: Results for the scenarios with OD error.

algorithm successfully converges to the correct solution. Yet, upon comparing results in Tab. 2 with those in Tab. 3, it is evident that the discrepancy introduced by the OD significantly affects the algorithm performance, particularly in terms of converging to the correct periodicity. As showed in Tab. 3, the number of correct solutions obtained when using SGP4 does not worsen with respect to the unperturbed case. Indeed, it is true that in the perturbed case errors due to the conversion from SGP4 to Keplerian elements are introduced. However, it could happen that these errors counteract those caused by OD noise. In such a case, if the fragment orbital state error resulting from OD leads to the selection of the wrong periodicity through the PoC metric, SGP4 conversion errors instead could simultaneously correctly guide the algorithm to the correct periodicity.
Concerning the scenario with OD error, the fragment-parent association always succeeds in the Keplerian case, even for fragments that converge to an incorrect solution. When using SGP4 instead, the 97.8% correctly achieves the association. Few analyses trigger the reliability alert, due to a low value of the peak contrast. Among the alerted simulations (respectively 5.7% for the unperturbed and 5.8% for the perturbed scenarios), the same percentage (69.2%) leads truly to a wrong solution, representing true positive cases. The rest are hence false positives. On the other hand, some of the failed fragments are not flagged, becoming hence false negatives. To conclude, in non-theoretical scenarios, the algorithm converges in most cases to the correct solution, but its robustness diminishes when the fragment and parent orbits exhibit similar orientations or have comparable shapes.

In order to assess the potential of CA techniques as a viable alternative to FRED method, this study compares the performance of the nominal scenarios in terms of estimation accuracy and computational demand. The results from FRED are taken from [5]. The computational time reported in the tables refer to a single fragment simulation.

	FRED	New routine
Correct solutions	92.8%	100%
Computational time	30 s	5 s

Table 4: Comparison with FRED: unperturbed scenario with no IOD error.

As evident from Tab. 4, Tab. 5 and Tab. 6, the number of correct solutions is generally higher with respect to those derived through FRED [5].

	FRED	New routine
Correct solutions	90%	100%
Computational time	5 min	54 s

Table 5: Comparison with FRED: perturbed scenario with no IOD error.

	FRED	New routine
Correct solutions	68.9%	83.1%
Computational time	5 min	56 s

Table 6: Comparison with FRED: perturbed scenario with IOD error.

Regarding the results of the scenario with OD error, their improvement may be due to the generation of the fragments mean state and covariance, which are obtained through a well-refined ROD, instead of a Keplerian-based method. In the simulations conducted with FRED, the fragment detection is performed only using an IOD based on a Keplerian approach [17].

4.5. Sensitivity Analysis

A sensitivity analysis is conducted on the perturbed scenario with OD error, to test the robustness of the routine to different conditions.

In all simulations described in Sec. 4.4, the detection of the fragments is set to happen 13 hours after t_0. Since in an operational context the first detection and OD process might happen later, t_{od} is shifted to two different values: 24 hours and 48 hours after the event. Extending the propagation window, the discrepancy at fragmentation epoch for the fragments mean state amplifies. The effect of a larger time elapsed between the event and the OD on the performance is hence investigated. Results are reported in Tab. 7. The more t_{od} is shifted from t_0, the lower becomes the number of fragments leading to a successful solution. Indeed, a longer

Time from t_0	Correct solutions	Selection failures	TCA failures	Alerts
+24 h	73.7%	26.3%	0%	5.8%
+48 h	56.6%	42.9%	0.5%	8.0%

Table 7: OD epoch sensitivity analysis. Perturbed scenario with nominal OD error.

propagation time implies a higher error on the state vector at t_0. The number of alerts produced in the simulation conducted with +24 h does not vary with respect to the case reported in Tab. 3. On the other hand, in the +48 h case, an increase in the percentage of estimates considered potentially inaccurate appears, probably following the significant rise of failed solutions. As proved by the simulation results presented in Sec. 4.4, the performance of the routine primarily depends on the accuracy of the OD process. A higher noise introduced by the sensor leads to larger uncertainties and discrepancy of the mean state with respect to the real one. Therefore, the robustness of the routine to a larger set of noise input is investigated. The noise level for the range is set constant to 30 m, while variations in the angular noise are introduced: from the nominal value of 0.01° to 0.02° and 0.05°. Results are reported in Tab. 8.

Angular noise	Correct solutions	Selection failures	TCA failures	Alerts
0.02°	77.8%	21.8%	0.4%	9.3%
0.05°	80.1%	19.0%	0.9%	14.2%

Table 8: Measurements noise sensitivity analysis. Perturbed scenario with nominal OD epoch.

With noises on the angular measurements that are higher with respect to the nominal case, the percentage of selection failures rises. The number of simulations providing an alert also increases with respect to the nominal case (Tab. 3). It is interesting to note that in the case of a 0.05° noise, despite it being higher, the routine performs slightly better compared to the case of 0.02° noise.

In all previous simulations the mean state of the parent object is never altered from the state acquired from the TLE, except during the splitting process required for the generation of the GMM. However, in real case scenarios, the TLEs are not fully accurate, and differences from the ground-truth shall be considered. Therefore, it is relevant to investigate the implications of a perturbed orbital state of the parent in input to the algorithm. The mismatch is introduced by randomly generating 10,000 samples of the parent state vector according to the distribution $\{\boldsymbol{x}^p, \boldsymbol{P}^p\}$, and retaining 10 of those, following their values of Mahalanobis distance and attempting to cover all levels of

perturbation. Ten simulations of the whole routine are hence repeated, providing each perturbed sample just derived. The results of all simulations are not reported in a specific table, but summarized as follows. In the theoretical case (unperturbed scenario without OD error) the number of correct estimates is always larger than 90%. In the perturbed scenario with OD error instead the percentage of successful solutions varies between 75.1% and 84.4%. For some samples the routine performs better than the nominal case, while for others, the percentage of correct solutions degrades. This is likely due to the combination of errors introduced by the error of the parent intial ephemeris and those introduced by the OD error of the fragment, and by the conversion from SGP4 elements to Cartesian coordinates and back. These factors may indeed influence and compensate each other in a way that is not entirely quantitatively interpretable. It is again confirmed that in most failed cases the algorithm converges to a wrong periodicity, while it occurs less frequently that the TCAs are evaluated inaccurately.

Previously, the same value of the ballistic coefficient B^* is used inside SGP4, both to generate the ground-truth and in the routine itself. Additionally, this value is set equal to zero, both for the parent and fragment. To introduce the role of atmospheric drag, as well as to assess the effects of the mismatching of B^* between the ground-truth generation and the routine itself, a new simulation is conducted. It is not always possible to accurately estimate the physical parameters of the object. Hence in the data set generation B^* is set to 0.00026658 for the parent, based on the last available TLE for Cosmos 1408, and $1e-04$ for the fragment, while in the algorithm both value are modified, multiplying them times $1e-02$. Results are reported in Tab. 9. The mismatching on the B^* values degrades slightly the number of correct solutions, with respect to the nominal case (Tab. 3), but the performance remains robust.

Correct solutions	Selection failures	TCA failures	Alerts
82.2%	17.3%	0.5%	5.8%

Table 9: Results for the perturbed scenario with OD error and mismatching on B^*.

5. Conclusions

This research is intended to contribute to the development of a new routine aimed at characterizing a fragmentation event.
An algorithm has been presented, which is able to detect the epoch of a fragmentation event, exploiting one ephemeris of the parent object and a single fragment orbital state, determined in the first hours after the event. In addition, a criterion for associating the fragment object to the broke-up spacecraft has been implemented to enable a comprehensive characterization of the event. Both the methodologies are based on techniques typical of CA theory.
Some significant conclusions can be drawn from the presented results. Firstly, the routine operates with a one hundred percent success rate if the scenario conditions are close to being ideal. When introducing perturbations, the results do not experience any degradation if again no error is applied in the OD. This is a positive outcome; however, numerical errors resulting from the conversion to SGP4 elements are reflected in the epoch estimates. These lead to errors still in the order of milliseconds, however slightly higher than in the Keplerian case. In non-theoretical scenarios, the algorithm converges in most cases to the correct solution, but its robustness diminishes when the fragment and parent orbits exhibit similar orientations or have comparable shapes. The refined MOID and TCA computations lead to accurate results even in cases where the data set is generated with OD errors. It appears that the majority of failures are attributed to convergence to the wrong periodicity, rather than to an inaccurate evaluation of TCA epochs. This is well observed in the sensitivity analysis conducted on the measurement noise, which degrades the results. However, this is also the result of an increased propagation time window from the event epoch to the detection epoch, which leads to the expansion of errors in the fragment states at the correct fragmentation epoch. Finally, the statistical representation based on GMM is beneficial in terms of computational time. Compared to the approach presented in [5], which aims at fragmentation epoch identification, the work here conducted al-

lows for a significant speeding up of the analysis on a single fragment.
Several developments can be conceived as future extensions of this work. Different propagation models (possibly high-fidelity) may be tested to introduce additional disturbances or customize their modeling. Evaluating the impact of a varying number of GMEs within a mixture on the routine outcomes holds theoretical interest.
Furthermore, a next crucial step involves the study of higher-order moments beyond the mean and variance, whose relevance is limited to Gaussian distributions. Future research may also focus on introducing existing methods of CA that inherently address the dilution problem (underestimation of the PoC for high uncertainties).
Finally, a significant step entails conducting the fragmentation epoch detection when a fragment is detected by a surveillance sensor, but no OD result can be derived. Indeed, it would be challenging but valuable to define an approach that leads to the epoch estimation directly within the measurements space.

References

[1] ESA Space Debris Office. Esa's space environment report 2023. Technical report, ESA ESOC, Robert-Bosch-Strasse 5 D-64293 Darmstadt Germany, 6 2023.

[2] Linda Dimare, Stefano Cicalò, Alessandro Rossi, Elisa Maria Alessi, and Giovanni B Valsecchi. In-orbit fragmentation characterization and parent bodies identification by means of orbital distances. In *First International Orbital Debris Conference*, volume 2109, page 6007, 2019.

[3] A Muciaccia, M Romano, C Colombo, et al. Detection and characterisation of in-orbit fragmentations over short and long periods of time. In *INTERNATIONAL ASTRONAUTICAL CONGRESS: IAC PROCEEDINGS*, pages 1–11, 2021.

[4] Roxana Larisa Andrișan, Alina Georgia Ioniță, Raúl Domínguez González, Noelia Sánchez Ortiz, Fernando Pina Caballero, and Holger Krag. Fragmentation event model and assessment tool (fremat) supporting on-orbit fragmentation analysis. In *7th European Conference on Space Debris*, 2016.

[5] Marco Felice Montaruli, Pierluigi Di Lizia, Emiliano Cordelli, Hélène Ma, and Jan Siminski. A stochastic approach to detect fragmentation epoch from a single fragment orbit determination. *Advances in Space Research*, 72(9):3713–3733, 2023. ISSN 0273-1177. doi: https://doi.org/10.1016/j.asr.2023.08.031. URL `https://www.sciencedirect.com/science/article/pii/S0273117723006798`.

[6] Nicholas L Johnson, Paula H Krisko, J-C Liou, and Phillip D Anz-Meador. Nasa's new breakup model of evolve 4.0. *Advances in Space Research*, 28(9):1377–1384, 2001.

[7] Jia-Sheng Li, Zhen Yang, and Ya-Zhong Luo. A review of space-object collision probability computation methods. *Astrodynamics*, 6(2):95–120, 2022.

[8] F Kenneth Chan. *Spacecraft collision probability*. American Institute of Aeronautics and Astronautics, Inc., 2008.

[9] Romain Serra, Denis Arzelier, Mioara Joldes, Jean-Bernard Lasserre, Aude Rondepierre, and Bruno Salvy. A new method to compute the probability of collision for short-term space encounters. In *AIAA/AAS Astrodynamics Specialist Conference*, page 4366, 2014.

[10] Salvatore Alfano. A numerical implementation of spherical object collision probability. *The Journal of the Astronautical Sciences*, 53:103–109, 2005.

[11] Victor P Osweiler. Covariance estimation and autocorrelation of norad two-line element sets. 2006.

[12] MF Montaruli, L Facchini, P Di Lizia, M Massari, Giuseppe Pupillo, GERMANO Bianchi, and Giovanni Naldi. Adaptive track estimation on a radar array system for space surveillance. *Acta Astronautica*, 198:111–123, 2022.

[13] G. F. Gronchi. On the stationary points of the squared distance between two ellipses with a common focus. *SIAM Journal on*

Scientific Computing, 24(1):61–80, January 2002. ISSN 1064-8275, 1095-7197. doi: 10.1137/S1064827500374170.

[14] Marcus J Holzinger, Daniel J Scheeres, and Kyle T Alfriend. Object correlation, maneuver detection, and characterization using control distance metrics. *Journal of Guidance, Control, and Dynamics*, 35(4): 1312–1325, 2012.

[15] Vivek Vittaldev et al. *Uncertainty propagation and conjunction assessment for resident space objects*. PhD thesis, 2015.

[16] A Muciaccia, L Facchini, MF Montaruli, G Purpura, R Detomaso, C Colombo, M Massari, P Di Lizia, A Di Cecco, L Salotti, et al. Observation and analysis of cosmos 1408 fragmentation. In *INTERNATIONAL ASTRONAUTICAL CONGRESS: IAC PROCEEDINGS*, pages 1–7, 2022.

[17] Jan Siminski. Techniques for assessing space object cataloguing performance during design of surveillance systems. In *6th International Conference on Astrodynamics Tools and Techniques (ICATT)*, pages 14–17, 2016.

[18] Marco Felice Montaruli, Giovanni Purpura, Riccardo Cipollone, Andrea De Vittori, Luca Facchini, Pierluigi Di Lizia, Mauro Massari, Moreno Peroni, Alessandro Panico, Andrea Cecchini, et al. A software suite for orbit determination in space surveillance and tracking applications. In *9th European Conference for Aerospace Sciences (EUCASS 2022)*, pages 1–12, 2022.